Conformational Exchange on the Microsecond Time Scale in α-Helix and β-Hairpin Peptides Measured by ^{13}C NMR Transverse Relaxation[†]

Irina Nesmelova,[‡] Alexei Krushelnitsky,[‡,§] Djaudat Idiyatullin,[‡] Francesco Blanco,[||] Marina Ramirez-Alvarado,[||] Vladimir A. Daragan,[‡] Luis Serrano,[||] and Kevin H. Mayo*[,‡]

Department of Biochemistry, Molecular Biology, and Biophysics, University of Minnesota Health Science Center, 321 Church Street, Minneapolis, Minnesota 55455, and European Molecular Biology Laboratory, Structures and Biocomputing Programme, Meyerhofstrasse 1, 69012 Heidelberg, Germany

ABSTRACT: ^{13}C-NMR relaxation experiments (T_1, T_2, $T_{1\rho}$, and NOE) were performed on selectively enriched residues in two peptides, one hydrophobic staple α-helix-forming peptide GFSKAELAKARAAKRGGY and one β-hairpin-forming peptide RGITVNGKTYGR, in water and in water/trifluoroethanol (TFE). Exchange contributions, R_{ex}, to spin−spin relaxation rates for $^{13}C_\alpha$ and $^{13}C_\beta$ groups were derived and were ascribed to be mainly due to peptide folding−unfolding. To evaluate the exchange time, τ_{ex}, from R_{ex}, the chemical shift difference between folded and unfolded states, $\Delta\delta$, and the populations of these states, p_i, were determined from the temperature dependence of ^{13}C chemical shifts. For both peptides, values for τ_{ex} fell in the 1 μs to 10 μs range. Under conditions where the peptides are most folded (water/ TFE, 5 °C), τ_{ex} values for all residues in each respective peptide were essentially the same, supporting the presence of a global folding−unfolding exchange process. Rounded-up average τ_{ex} values were 4 μs for the helix peptide and 9 μs for the hairpin peptide. This 2−3-fold difference in exchange times between helix and hairpin peptides is consistent with that observed for folding−unfolding of other small peptides.

It is well known that proteins and peptides undergo internal motions over a wide range of time scales from picoseconds to milliseconds and longer. NMR[1] spectroscopy has been used extensively to investigate many types of internal motions. Fast motions falling in the picosecond to nanosecond range generally arise from motions of individual bonds (^{15}N−H or ^{13}C−H) or small groups of atoms (e.g., CH$_2$ or CH$_3$) that are faster than the overall tumbling time of the molecule. These fast motions contribute to NMR relaxation parameters, such as the spin−lattice (longitudinal) relaxation rate, R_1, the nuclear Overhauser effect (NOE), the spin−spin (transverse) relaxation rate, R_2, and the rotating frame spin−lattice relaxation rate, $R_{1\rho}$. Derivation of amplitude (order parameter) and frequency (correlation time) of these fast motions in proteins and peptides is usually based on the analysis of these NMR relaxation parameters.

Internal motions of larger groups of atoms, correlated motions of several residues, segmental motions, and the like usually occur on the nanosecond to microsecond time scales, whereas conformational reorganization of the entire molecule, like folding−unfolding, occurs on the slower time scale of microseconds to milliseconds. Internal motions occurring on these time scales contribute primarily to the transverse relaxation rate that results from dephasing of spin coherences caused by random jumps between or among states of nuclei having different chemical environments such that the NMR line for each state will have a different chemical shift, ν. This process is referred to as chemical exchange, and the motional time is given by the exchange lifetime, τ_{ex}. To simplify derivation of slower motions from NMR relaxation data, it is usually assumed that exchange occurs between two states, a and b. When the exchange process falls within the slow or intermediate time regime on the chemical shift time scale, i.e., $(2\pi\Delta\nu\tau_{ex})^2 \gg 1$ or ~ 1 ($\Delta\nu$ is the chemical shift difference between two states), it is possible to derive parameters that characterize the chemical exchange process, i.e., τ_{ex} and the populations of each conformational state, p_a and p_b, from analysis of the temperature dependence of line shapes or from the dependence of the transverse relaxation rate on the effective field strength, $\omega_1 = \gamma B_1$ (*1*). On the other hand, if the exchange between the two states is fast on the chemical shift time scale, $(2\pi\Delta\nu\tau_{ex})^2 \ll 1$, then only one single, narrow resonance is observed at the chemical shift position that is the weighted average of the chemical shifts of both states. In this fast exchange regime, the averaged resonance is independent of the effective field, B_1, which makes analysis of the exchange process complicated. In this case, it is impossible to independently obtain the exchange time and the populations in the different states from analysis

---

* Address correspondence to this author. Tel: 612-625-9968. Fax: 612-624-5121. E-mail: mayox001@maroon.tc.umn.edu.

[‡] University of Minnesota Health Science Center.

[§] Current address: Institute of Biophysics, Russian Academy of Sciences, Kazan, Russia.

[||] European Molecular Biology Laboratory.

[1] Abbreviations: NMR, nuclear magnetic resonance; NOE, nuclear Overhauser effect; R_1, spin−lattice (longitudinal) relaxation rate (=1/T_1); R_2, spin−spin (transverse) relaxation rate (=1/T_2); $R_{1\rho}$, rotating frame spin−lattice relaxation rate; R_{ex}, exchange contribution to R_2; τ_{ex}, exchange time.

of the transverse relaxation rate, R_2, and its temperature and/ or field dependence. To estimate τ_{ex}, one needs to use a value for the chemical shift difference, $\Delta\nu$, and the populations of the two states, p_a and p_b, from independent measurements.

Mandel et al. (2), for example, used NMR spectroscopy to demonstrate that the upper limit for conformational exchange in RNase H is 10 μs. For this, these authors merely assumed that the chemical shift difference, $\Delta\nu$, between folded and unfolded conformations was 2 ppm. For an alanine-based helix-forming peptide, Thompson et al. (3) found that the helix folding time was about 1 μs. For cytochrome c, the shortest folding time was found to be 130 μs (4). Folding times for β-hairpin/sheet formation are usually longer than those for folding of helical peptides. For a 20-residue peptide designed to fold into a monomeric three-stranded antiparallel β-sheet in aqueous solution, the folding time for β-sheet formation was estimated from NMR measurements to be in the range 4−14 μs at 10 °C (5). Folding of a 16-residue β-hairpin has been shown to occur in about 6 μs at room temperature (6).

Short linear peptides usually exist in solution as a distribution of transient, rapidly interconverting conformations making structural characterization using NMR problematic, given the presence of few, if any, long-range, conformationally informative ^{1}H−^{1}H NOEs, J-coupling constants, or chemical shifts. Several peptides, however, have been designed or identified as having at least some structure under certain solution conditions. In the present study, two model peptides, one helical and one hairpin, have been investigated using ^{13}C-NMR relaxation methods to derive the range of possible folding−unfolding exchange times (τ_{ex}) from the exchange contribution, R_{ex}, to R_2. Even though folding−unfolding may occur via multiple steps, a two-state process was assumed to simplify analysis of NMR exchange data, which, in any event, would not allow discrimination between two-state and multiple-state exchange processes. For this analysis, chemical shift differences and populations of different states have been estimated from analysis of the temperature dependence of chemical shifts. The hairpin peptide being studied (RGITVNGKTYGR) is partially folded under a variety of solution conditions (7). NOE-based distance geometry calculations demonstrate formation of a β-hairpin from residue 3 to residue 10 and centered at NG (Figure 1). In this peptide, seven residues, G2, I3, T4, V5, G7, Y10, and G11, were selectively and uniformly ^{13}C-enriched. While G2 and G11 monitor dynamics at the unstructured termini, G7 is part of the β-turn, and the two remaining residues with bulky side chains, V5 and Y10, are positioned on the same face of a short β-sheet in the hairpin and show cross-strand NOEs. The second peptide being studied is a short linear peptide 18mer, GFSKAELAKARAAKRGGY, which has been shown to fold in an α-helical conformation stabilized by formation of a hydrophobic staple motif (see Figure 1) (8). In this peptide, five residues, F2, A5, L7, A8, and A10, were selectively and uniformly ^{13}C-enriched. For this peptide in water at 5 °C, numerous conformationally constraining, long-range ^{1}H NOEs have been observed, and distance geometry calculations using these NOE constraints have demonstrated formation of a turn centered at SK which leads into an α-helix conformation from A5 through A12. The C-terminal portion appears to form a nascent helix and is much less structured. From analysis of chemical shifts,
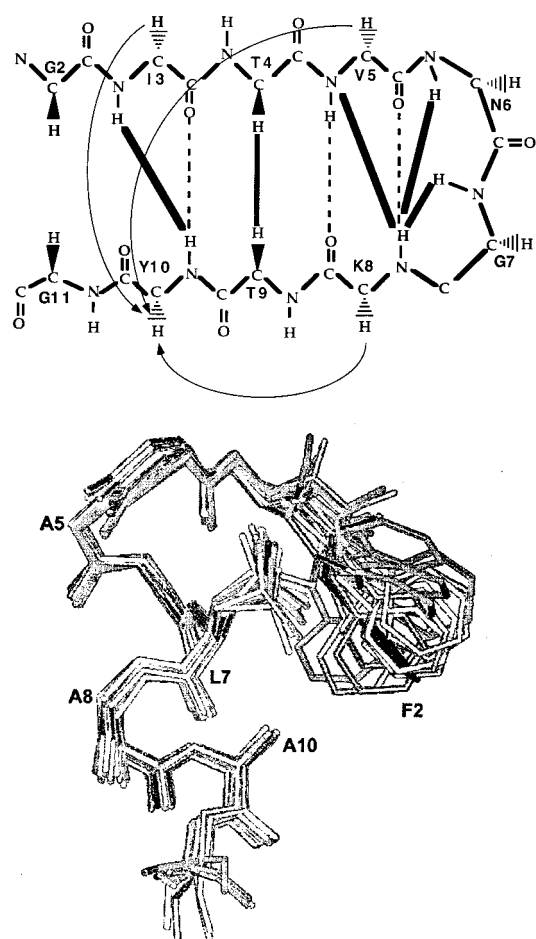

FIGURE 1: NMR-derived structures for α-helix (bottom) and β-hairpin (top) peptides. For the helical peptide, the superposition of the structures is shown, whereas for the hairpin peptide, the general backbone fold is shown with interresidue NOEs indicated.

$^3J_{\alpha N}$ coupling constants, NOE intensities, and CD data, the α-helix population is most significant at 5 °C, i.e., about 50%.

MATERIALS AND METHODS

Peptides. Both peptides, one helix-forming peptide GF-SKAELAKARAAKRGGY and one β-hairpin-forming peptide RGITVNGKTYGR, were synthesized on a Milligen/Millipore Excell peptide synthesizer or on an Applied Biosystems 431A peptide synthesizer (9) using Fmoc solid-phase methodology. Peptides were isotopically enriched with uniformly ^{13}C-labeled amino acids (CIL, Cambridge) at residues F2, A5, L7, A8, and A10 in the α-helix-forming peptide and at residues G2, I3, T4, V5, G7, Y10, and G11 in the β-hairpin-forming peptide. Peptides were purified by HPLC using a linear acetonitrile/water gradient, and the purity was checked by analytical HPLC on a C_{18} Bondclone (Phenomenex) column and fast atom bombardment mass spectrometry. The peptide concentration was determined from the dry weight of freeze-dried samples. To avoid ^{13}C resonance overlap, separate peptides, each with different residues enriched in ^{13}C, were produced: three peptides for the helix (F2−A8, A5−L7, and A10) and five peptides for the hairpin (G2-V5, I3, T4, G7−Y10, and G11). For assurance that peptides behaved the same in solution, ^{1}H-NMR and CD spectra were acquired on each peptide and were found to be identical.

NMR Relaxation Measurements. For ^{13}C-NMR relaxation measurements, freeze-dried peptides were dissolved in D_2O or in 65/35 (v/v) D_2O/trifluoroethanol (TFE). Peptide concentration, determined from the dry weight of freeze-dried samples, was 15 mg/mL. The pH was adjusted to 6 by adding microliter quantities of NaOD or DCl. NMR experiments were performed on Varian Inova-500, -600, and -800 NMR spectrometers equipped with triple-resonance probes and on a Bruker AM-250 NMR spectrometer equipped with a ^{13}C direct-observe probe. The temperature was varied from -8 to 65 °C.

Spin−lattice relaxation rates, R_1, were determined by using the direct homonuclear inversion−recovery method with a composite 180° ($90°_x-180°_y-90°_x$) pulse with broad-band ^{1}H-decoupling GARP (*10*). The number of acquisitions was chosen to give a signal-to-noise ratio greater than 10 and, therefore, was varied from 200 to 1000. Ten to fifteen time-incremented (partially relaxed) spectra were routinely acquired for each relaxation measurement. Relaxation rates were determined as described by Daragan et al. (*11*). {^{1}H}-^{13}C NOE coefficients were measured by using the standard gated decoupling technique.

^{13}C spin−spin relaxation rates, R_2, were measured as a function of the effective field strength, B_{1eff}, using Carr−Parcell−Meiboom−Gill (CPMG) spin−echo and off-resonance spin-lock experiments. CPMG experiments were performed using the pulse sequence described by Farrow et al. (*12*) with a few minor modifications. The first modification in the CPMG pulse train consisted of applying soft rectangular 180° pulses (714−1250 Hz) exactly on the resonance frequency of a given nucleus. Selective excitation avoids modulation of the spin−echo decay by *J*-coupling (*13−15*), which occurs when nuclei have at least one bonded ^{13}C-labeled neighbor. The second modification involved the use of narrow-band, constant irradiation proton decoupling during the relaxation period because wide-band decoupling schemes such as WALTZ and GARP do not work well for *J*-coupled nuclei (*16*, *17*). τ_{cp} was varied from 150 to 400 μs. Relaxation times were determined from the slope of the relaxation decay using 15 points.

Off-resonance rotating frame, $T_{1\rho}$, relaxation experiments were performed using pulse sequences described by Zinn-Justin et al. (*18*) and by Mulder et al. (*19*). The same modifications (soft pulses and narrow band decoupling) as were done for CPMG measurements were employed. The strength of the effective spin-lock field was determined as $B_{1eff} = [\Delta^2 + (B_1)^2]^{1/2}$, where Δ is the resonance offset of the applied B_1 field. Δ was varied from 400 to 5280 Hz. The duration of the spin-lock pulse (the relaxation period) was varied from 0 to 300 ms to yield 15 points on the relaxation decay curve. In $T_{1\rho}$ experiments, the transverse relaxation rate, R_2 ($=1/T_2$), was obtained from the equation:

$$R_{1\rho} = R_1 \cos^2\theta + R_2 \sin^2\theta \quad (1)$$

where $R_{1\rho}$ and R_1 are the longitudinal relaxation rates in the rotating and laboratory frames, respectively, θ is the angle between the effective spin-lock field and the B_0 field. θ, as well as the amplitude of the effective spin-lock field, is regulated by the combination of the resonance offset of the applied B_1 field and its strength (*18*). In our experiments, θ was optimal between 30° and 50°.

Chemical exchange contributions, R_{ex}, to spin−spin relaxation rates, R_2, were obtained using a Monte Carlo minimization protocol (*20*) which minimized the function (*11*):

$$\chi^2 = \Sigma_i[(R^i_{1exp} - R^i_{1theor})/R^i_{1exp}]^2 + [(R^i_{2exp} - R^i_{2theor})/R^i_{2exp}]^2 + [(\text{NOE}^i_{exp} - \text{NOE}^i_{theor})/\text{NOE}^i_{exp}]^2 \quad (2)$$

where R^i_{1exp}, R^i_{2exp}, and NOE^i_{exp} are the experimental values and R^i_{1theor}, R^i_{2theor}, and NOE^i_{theor} are the calculated values of the NMR relaxation parameters which can be expressed in terms of spectral densities:

$$R_1 = \frac{1}{10}k_{dd}[J(\omega_C - \omega_H) + 3J(\omega_C) + 6J(\omega_C + \omega_H)] + \frac{2}{15}\Delta\sigma^2\omega_C^2 J(\omega_C) \quad (3a)$$

$$R_2 = R_{2dd} + R_{ex} \quad (3b)$$

where

$$R_{2dd} = \frac{1}{20}k_{dd}[J(\omega_C - \omega_H) + 3J(\omega_C) + 6J(\omega_C + \omega_H) + 4J(0) + 6J(\omega_H)] + \frac{1}{45}\Delta\sigma^2\omega_C^2[4J(0) + 3J(\omega_C)]$$

$$\text{NOE} = 1 + \frac{\gamma_H}{\gamma_C}\frac{k_{dd}[6J(\omega_C + \omega_H) - J(\omega_C - \omega_H)]}{W_1} \quad (3c)$$

where R_{2dd} is the ^{13}C−^{1}H dipole−dipole contribution to R_2, $k_{dd} = n\gamma_C^2\gamma_H^2\hbar^2/r^6_{CH}$, γ_C and γ_H are the magnetogyric ratios for ^{13}C and ^{1}H nuclei, respectively, $\hbar$ is the Planck constant, r_{CH} is the length of CH bond, and n is the number of attached protons. Chemical shift anisotropy, $\Delta\sigma$, was estimated to be -25 ppm for ^{13}C (*21*). Since contributions from ^{13}C CSA to the relaxation rates are much smaller (less than ∼5%) than contributions from ^{13}C−^{1}H dipole−dipole interactions even at high field (*21*), this term was neglected during data analysis. In addition, dipolar coupling between adjacent carbons in uniformly ^{13}C-labeled amino acids can contribute to carbon relaxation rates (*22*). In general, the effect is greater for molecules exhibiting larger overall tumbling correlation times and at higher magnetic fields. Because of this, relaxation data were corrected by assuming that contributions from C−H and C−C spectral densities were equal. This reasonable assumption contributed less than 2% to the error in calculating relaxation rates. Using this approach, it was found that the contribution from ^{13}C−^{13}C dipole interactions was less than about 5% for these short peptides in aqueous solution at 30 °C. This contribution increased somewhat at lower temperatures and was maximally 11% in TFE solution at 5 °C due to larger overall tumbling times resulting from increased solution viscosity.

During minimization of eq 2, the summation was performed over all the NMR frequencies for which data were available. In this analysis, no specific model is used for the spectral density function; rather the spectral density function is directly fit during the minimization protocol as discussed by Mayo et al. (*20*). The R_{ex} term was taken to be proportional to the Larmor frequency squared. Recently, Millet et al. (*23*) demonstrated that this usual assumption,

i.e., at the fast exchange limit R_{ex} scales quadratically with the magnetic field, may be incorrect if the population of one exchanging state is greater than 70% and the product $(2\pi\Delta\nu\tau_{ex})^2$ is less than 1 but not that much less than 1; i.e., the fast exchange condition is not fully met. Even though folded−unfolded state populations of these helix and hairpin peptides can be greater than 70%, it is evident that when their exchange times, τ_{ex}, are in the $1-10\ \mu s$ range with $\Delta\nu = 400$ Hz, $(2\pi\Delta\nu\tau_{ex})^2$ is 6.3×10^{-6} to 6.3×10^{-4}. These values are much, much less than 1, indicating that the fast exchange condition would be fulfilled. Even with τ_{ex} of 100 μs, $(2\pi\Delta\nu\tau_{ex})^2$ would be 6×10^{-2}. For the peptides studied here, therefore, taking R_{ex} proportional to the square of the Larmor frequency is valid.

Values for R_{ex} were then used to derive exchange times, τ_{ex}. Although a multistate exchange process could not be ruled out, analysis was greatly simplified by using a two-state model. For a two-site exchange process occurring on the fast chemical shift time scale, R_{ex} measured by using the Carr−Purcell−Meiboom−Gill (CPMG) pulse sequence can be approximated (*24*) as

$$R_{ex} = p_a p_b \delta\omega^2 \tau_{ex}[1 - 2(\tau_{ex}/\tau_{CPMG}) \tanh(0.5\tau_{CPMG}/\tau_{ex})] \quad (4)$$

where p_a and p_b are the relative exchange site populations, $\delta\omega = 2\pi\Delta\nu$, with $\Delta\nu$ being the chemical shift difference between the two states, τ_{ex} is the time constant for the exchange process, and τ_{CPMG} is the time interval between 180° pulses in the CPMG pulse sequence. For $T_{1\rho}$ measurements (*25*), the exchange contribution is given by

$$R_{ex} = \delta\omega^2 p_a p_b \tau_{ex}/[1 + (\omega_1\tau_{ex})^2] \quad (5)$$

Folded State Populations and Chemical Shift Differences. To determine chemical shifts, proton-decoupled ^{13}C spectra were acquired with a resolution of 0.5 Hz. Chemical shifts were expressed in absolute frequency with no internal reference. The temperature dependence of chemical shifts was analyzed by assuming fast exchange between two states (folded and random coil):

$$\nu_{obs} = p_h\nu_h + (1 - p_h)\nu_c \quad (6)$$

ν_h and p_h are the carbon chemical shift and the population of peptide, respectively, in either the α-helix or β-hairpin conformation; ν_c is the carbon chemical shift in the random coil state. Both populations and chemical shifts are temperature dependent. Since the α-helix (or β-hairpin)−coil transition is a cooperative process, the temperature dependence of the peptide population in each conformational state is described by a sigmoidal curve (*26*) such that

$$\ln K_{ex} = \ln[(1 - p_h)/p_h] = 2(T - T_m)/\Delta T \quad (7)$$

K_{ex} is the equilibrium constant for the conformational transition, T_m is the midpoint of the transition, and ΔT is the width of the transition. The temperature dependence of chemical shifts within structured and random coil conformations is assumed to be linear:

$$\nu_h = \left(\frac{d\nu}{dT}\right)_{h,c} T + \nu_{h,0} \quad \text{and} \quad \nu_c = \left(\frac{d\nu}{dT}\right)_{h,c} T + \nu_{c,0} \quad (8)$$

Following substitution of ν_h and ν_c (from eq 8) and p_h (from eq 7) into eq 6, the temperature dependence of the observed chemical shift, ν_{obs}, can be expressed as

$$\nu_{obs} = \frac{1}{1 + \exp\left(2\dfrac{T - T_m}{\Delta T}\right)}\left[\left(\frac{d\nu}{dT}\right)_{h,c} T + \nu_{h,0}\right] + \frac{\exp\left(2\dfrac{T - T_m}{\Delta T}\right)}{1 + \exp\left(2\dfrac{T - T_m}{\Delta T}\right)}\left[\left(\frac{d\nu}{dT}\right)_{h,c} T + \nu_{c,0}\right] \quad (9)$$

Experimental temperature dependencies of carbon chemical shifs were fit to eq 9 using the Marquardt−Levenberg algorithm for nonlinear regression. To remove the temperature dependence of the deuterium lock frequency from the temperature dependence of ν_{obs}, the temperature dependence of the deuterium lock frequency was determined separately for water and for exactly the same mixture of water/TFE solution using DSS as a reference, and the temperature dependence was approximated using a second-order polynomial and was subtracted from that of ν_{obs}. To reduce the number of fitting parameters, the temperature dependence of chemical shifts in structured and coiled states was assumed to be the same, i.e., have the same slope. The final equation had five fitting parameters: T_m, ΔT, $\nu_{h,0}$, $\nu_{c,0}$, and $(d\nu/dT)_{h,c}$. Since the folding−unfolding process was assumed to be global, T_m and ΔT should be the same for all residues. Both α-carbon and carbonyl carbon chemical shifts were fit in order to provide chemical shift differences and populations of structured and random coil conformations.

RESULTS

^{13}C−H relaxation experiments (T_1, T_2, $T_{1\rho}$, and NOE) were performed on isotopically enriched backbone and side-chain groups of residues F2, A5, L7, A8, and A10 in the α-helix-forming peptide GFSKAELAKARAAKRGGY and of residues G2, I3, T4, V5, G7, Y10, and G11 in the β-hairpin-forming peptide RGITVNGKTYGR in water and in water/TFE. T_1 and NOE data were acquired at four Larmor frequencies (^{13}C frequencies of 63, 125, 150, and 201 MHz), whereas T_2 and $T_{1\rho}$ data were measured at 125 and 201 MHz. In deriving the exchange contribution, R_{ex}, to R_2 ($=1/T_2$), relaxation data acquired at 201 MHz (for ^{13}C) were most useful because R_{ex} contributes more to R_2 at higher Larmor frequencies. Data were also acquired at temperatures from 5 °C, where the peptides are mostly structured, to 30 °C, where the peptides are mostly unstructured. To exemplify the quality of relaxation data, Figure 2 shows the temperature dependence of R_2 and Figure 3 shows the temperature dependence of selective R_1 ($=1/T_1$) and NOE data from both peptides. For the helical peptide, R_2 (Figure 2) for residues within the helix segment (A5, L7, A8, and A10) are nearly the same, whereas R_2 for residue F2 is significantly smaller, consistent with F2 being positioned at the more mobile N-terminus of the peptide. For the hairpin peptide, R_2 values for most residues are nearly the same and follow the same temperature trend. For both peptides, R_1 and NOE data (Figure 3) behave similarly, demonstrating comparable
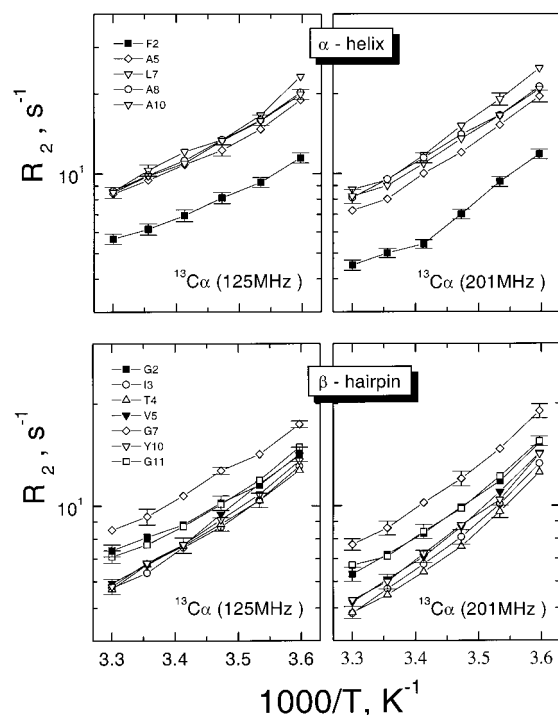
FIGURE 2: Backbone $^{13}C_\alpha$ spin−spin relaxation rates, R_2, for both β-hairpin (bottom panels) and α-helix (top panels) peptides in water/TFE are plotted versus the inverse temperature in K^{-1}. Data are presented for two ^{13}C Larmor frequencies, 125 and 201 MHz. Legends for the symbols identifying residues in each peptide are presented in the figure.
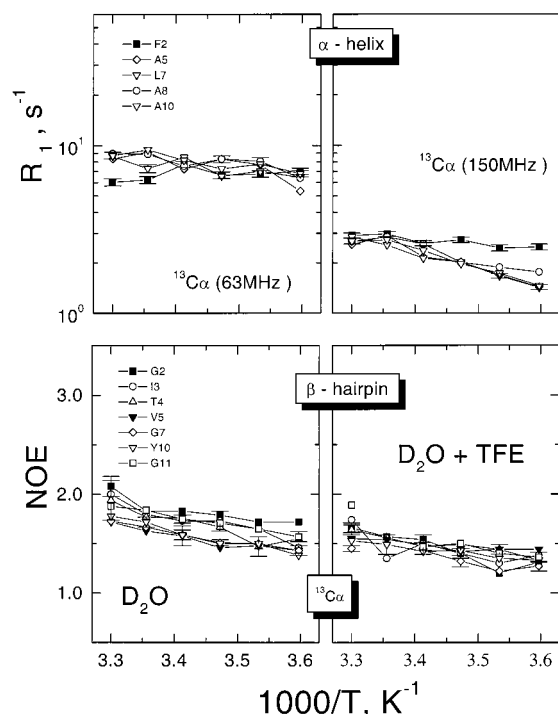

FIGURE 3: Backbone $^{13}C_\alpha$ spin−lattice relaxation rates, R_1, for the α-helix peptide in water/TFE (top panels) and {^1H}-$^{13}C_\alpha$ nuclear Overhauser effects (NOEs) for the β-hairpin peptide in water and water/TFE (bottom panels) are plotted versus the inverse temperature in K^{-1}. Data are presented for two ^{13}C Larmor frequencies, 63 and 150 MHz, in the top panels and for a ^{13}C Larmor frequency of 150 MHz in the bottom panels. Legends for the symbols identifying residues in each peptide are presented in the figure.

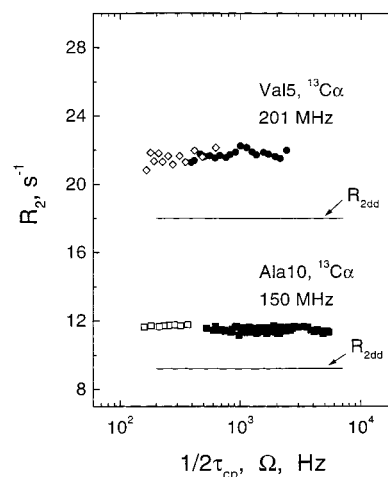temperature trends and magnitudes over all labeled sites within each peptide.

FIGURE 4: $^{13}C_\alpha$ spin−spin relaxation rates, R_2, measured by using the CPMG pulse sequence at various delays between 180° pulses are shown as open symbols, along with data from off-resonance $T_{1\rho}$ experiments performed at various spin-locking fields (solid symbols). τ_{cp} is the time delay between 180° pulses in the CPMG sequence; Ω is the effective spin-locking frequency, $\Omega = [\Delta^2 + (\gamma H_1)^2]^{0.5}$, where Δ is the resonance offset of the applied B_1 field. Data are shown for the α-helix peptide in water at 5 °C and for the β-hairpin peptide in water at 5 °C (^1H resonance frequency of 800 MHz). Solid lines indicate the dipole−dipole contributions to the spin−spin relaxation rate, which was obtained from the minimization protocol described in the Materials and Methods section.

As will be presented later, there is a clear exchange contribution, R_{ex}, to R_2. To establish limits on the frequency or time range in which the exchange process could be occurring, the dependence of R_2 was investigated as a function of the spacing between 180° pulses in the CPMG pulse sequence and as a function of the field-lock strength in off-resonance $T_{1\rho}$ experiments. For α-helix and β-hairpin peptides, typical examples of the frequency dispersion in R_2 are shown in Figure 4. Although data are presented for only one residue in each peptide, essentially the same trends were observed for all residues investigated. Since spin-lock frequencies above a few kilohertz could not be achieved experimentally and the curve for R_2 over the accessible range of frequencies is flat, one cannot conclude from these data alone that any exchange process is occurring. However, R_2 is larger than the dipole−dipole contribution, R_{2dd}, to spin−spin relaxation, R_2, which is shown as solid lines in the figure. R_{2dd} was calculated during the minimization protocol using eq 3 (see Materials and Methods section). Given this inequality, an exchange process must be contributing to the observed transverse relaxation rate, R_2. Moreover, the lack of frequency dependence in R_2 from 160 to 5280 Hz (see Figure 4) indicates the exchange time limits (6 ms to 190 μs) within which dynamic processes are not occurring. This, in turn, indicates that an exchange process is occurring on the sub-millisecond time scale, with an exchange time of less than 190 μs. This is consistent with the observation that, under all conditions investigated, only one ^{13}C resonance was observed for each labeled carbon atom in either peptide. Chemical exchange, therefore, is occurring either on the fast exchange time scale or, alternatively, on the intermediate or slow exchange time scales with one state having the major population since no signals were observed from states having a minor population (27). Folded state populations for these peptides were initially estimated from analysis of circular dichroism (CD) data. Since at 5 °C both folded and random
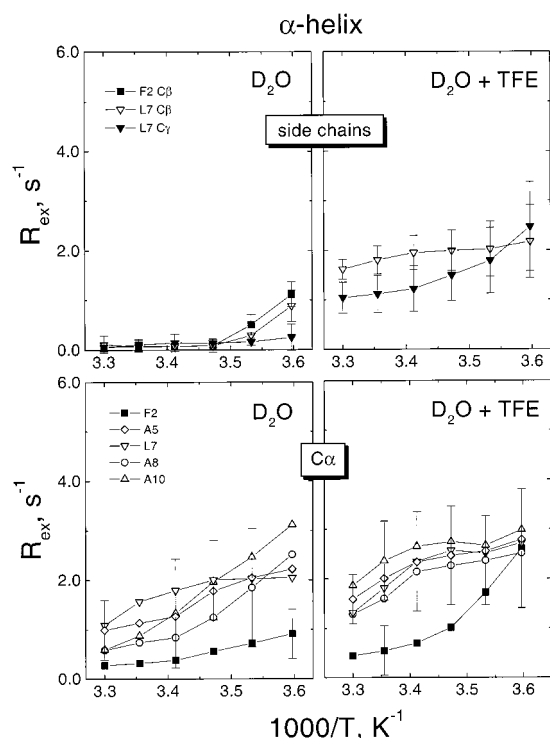
FIGURE 5: The temperature dependencies of the chemical exchange contributions, R_{ex}, to spin−spin relaxation rates are shown for data acquired at 201 MHz for backbone $^{13}C_\alpha$ and for some side-chain C_β and C_γ nuclei of residues in the α-helix peptide in water and in water/TFE. Vertical bars indicate errors in determining R_{ex}. These errors were determined by varying relaxation terms (R_1, R_2, and NOE) within their experimental error range and recalculating R_{ex} as described in the Materials and Methods section. In effect, this gives a range of acceptable values for R_{ex}.

FIGURE 6: The temperature dependencies of the chemical exchange contributions, R_{ex}, to spin−spin relaxation rates are shown for data acquired at 201 MHz for backbone $^{13}C_\alpha$ nuclei and for some side-chain C_β nuclei of the residues in the β-hairpin peptide in water and in water/TFE. Vertical bars indicate errors in determining R_{ex}. These errors were determined by varying relaxation terms (R_1, R_2, and NOE) within their experimental error range and recalculating R_{ex} as described in the Materials and Methods section. In effect, this gives a range of acceptable values for R_{ex}.

coil states have comparable populations, 50% folded in the α-helix peptide (*8*) and 35% folded in the β-hairpin peptide (*7*), it was concluded that exchange must be fast on the chemical shift time scale.

The exchange contribution, R_{ex}, to R_2 for individual sites was determined as described in the Materials and Methods section by fitting all relaxation data acquired for that particular site. Values for R_{ex} are plotted as a function of the inverse temperature in Figures 5 and 6 for the helix and hairpin peptides, respectively, in water and in water/TFE. In both figures, the bottom panels are for $^{13}C_\alpha$-labeled sites and the top panels are for $^{13}C_\beta$- or $^{13}C_\gamma$-labeled sites. For both peptides in water, R_{ex} values for $^{13}C_\beta$- or $^{13}C_\gamma$-labeled sites were mostly 0 or were very small, whereas in water/TFE, they became comparable to those for $^{13}C_\alpha$-labeled sites. R_{ex} values for $^{13}CH_3$ groups were 0 or very small both in water and in water/TFE and, therefore, will not be discussed further. For those ^{13}C-labeled sites indicated in Figures 5 and 6, the increase in R_{ex} as the temperature is decreased reflects the trend in the exchange time, τ_{ex} (eqs 3 and 4), which is usually greater at lower temperature; i.e., the exchange process is slower. Note, however, that the temperature dependence in R_{ex} may not be the same as that for τ_{ex} because the populations in different states are also temperature dependent. Addition of TFE also tends to increase R_{ex}, i.e., slow the exchange process. Since R_{ex} for backbone C_α and side-chain C_β/C_γ groups of both peptides at low temperature and in the presence of TFE, are, within error, the same, this exchange process is probably global in
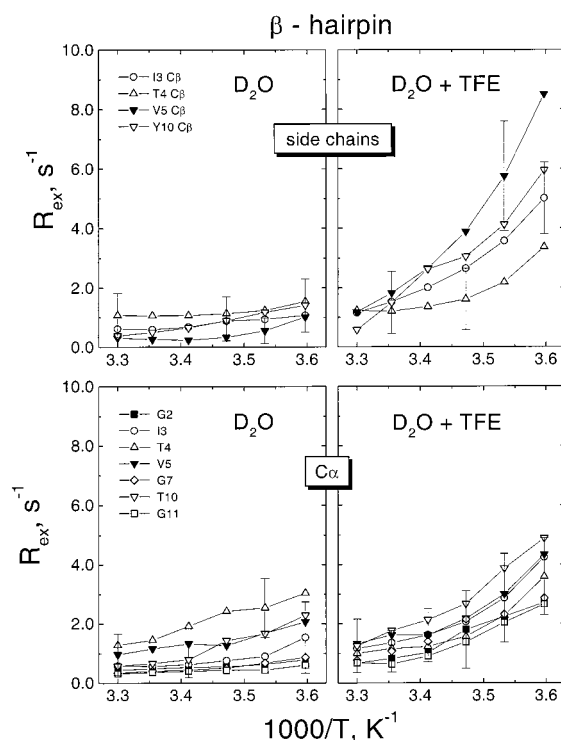
nature and is most likely due to folding−unfolding. For the hairpin peptide, R_{ex} values are essentially the same for all residues at any temperature (Figure 6). With the exception of F2, residues in the helix peptide also show the same R_{ex} values at any given temperature (Figure 5). The fact that R_{ex} for F2 behaves differently may be explained by it being at the more mobile N-terminus. In any event, in water/TFE at 5 °C where the peptide is most folded, R_{ex} for F2 is the same as for all other residues in the helix peptide.

To better understand the exchange processes, knowledge of the exchange time, τ_{ex}, is required. To a first approximation, chemical exchange events often can be explained by using a two-state model which not only simplifies data analysis but, given the experimental and fitting errors discussed below, was deemed appropriate here for deriving values for τ_{ex}. For two-site exchange, τ_{ex} can be calculated from R_{ex} by using eq 4 or 5 with values for $\Delta\nu$, the chemical shift difference between conformational states, and p_i, the populations in each state. Since the fast exchange limit is observed on the chemical shift time scale and R_2 is independent of the spacing between 180° pulses in CPMG and the field-lock strength in off-resonance $T_{1\rho}$ experiments (see Figure 4), eqs 4 and 5 can be simplified to

$$R_{ex} = \delta\omega^2 p_a p_b \tau_{ex} \qquad (10)$$

Initially, upper and lower limits for τ_{ex} were estimated. Since $T_{1\rho}$ data (Figure 4) indicate an exchange time cutoff of 190 μs, τ_{ex} must be less than that value. Reasonable limits for
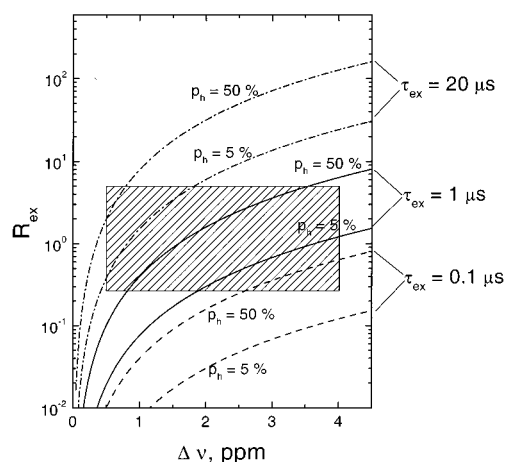
FIGURE 7: The theoretical chemical exchange contribution, R_{ex}, to spin−spin relaxation rates is plotted vs the ^{13}C chemical shift difference, $\Delta\delta$, between folded and unfolded states of a peptide. Calculations have been done for three different exchange times, τ_{ex}, and the shaded box illustrates the most probable region in which τ_{ex} should be for these systems, given the magnitudes of R_{ex} shown in the previous figures.

^{13}C $\Delta\nu$ between folded (α-helix and β-hairpin) and random coil states have usually been found to be between 100 and 800 Hz (0.5 and 4 ppm, respectively, at 201 MHz) (28). This, together with R_{ex} found for these peptides (Figures 5 and 6), restricts the region wherein τ_{ex} should lie. This region is indicated in Figure 7 by the shaded area. By selecting values of τ_{ex} according to the condition that the dependence of R_{ex} should pass through the shaded area, the limits for τ_{ex} must be between 20 μs (dashed−dotted lines) and 0.1 μs (dashed lines). The R_{ex} dependencies on $\Delta\nu$ have been calculated for two populations (p_h of 50% and 5%). These two populations were chosen because $p_h = 50\%$ gives the maximum value of the product $p_h (1 - p_h)$, whereas $p_h = 5\%$ (or 95%) is close to the maximally reasonable population at which one can expect to experimentally observe an exchange contribution to R_2. Therefore, for each particular value of τ_{ex}, all possible dependencies of R_{ex} at the population p_h between 5% and 50% will lie between these two curves which were calculated for $p_h = 50\%$ and $p_h = 5\%$. At $p_h = 50\%$, the curve for $\tau_{ex} = 1$ μs falls mostly within the most probable, shaded area.

For derivation of actual τ_{ex} values from R_{ex}, it is necessary to know p_h, p_c, and $\Delta\nu$. Although folded-state populations have been given in the literature for both hairpin (7, 29) and helix (8) peptides, all three terms were independently derived using eq 9 with the temperature dependence of chemical shifts for backbone C_α and carbonyls which yielded similar results. The best fits to eq 9 can be obtained when the experimentally available temperature range covers the transition temperature, T_m, between folded and unfolded states, as well as the width of the temperature transition, ΔT. The lowest temperature that was accessible experimentally was −2 °C in water and −8 °C in water/TFE. For the helix peptide in water, for example, T_m could be accurately determined because it was well above this low-temperature cutoff, i.e., +8 ± 3 °C [14 °C from the literature (4)], and ΔT was 38 ± 6 °C (see Table 1). To exemplify these data and fits using eq 9, Figure 8 plots the temperature dependence of $^{13}C_\alpha$ chemical shifts for a few residues in each peptide. The actual data are given as open symbols, and the solid

Table 1: Parameters for Derivation of Exchange Times for Helix and Hairpin Peptides

residue	$\Delta\nu$, Hz	ΔT, °C	T_m, °C	p_h, % 5 °C	30 °C
		Helix Peptide in Water			
F2	225[a]	38 ± 6	9 ± 3	55 ± 4	24 ± 4
A5	200 ± 14	38 ± 6	9 ± 3	55 ± 4	24 ± 4
L7	256 ± 18	38 ± 6	9 ± 3	55 ± 4	24 ± 4
A8	254 ± 18	38 ± 6	9 ± 3	55 ± 4	24 ± 4
A10	191 ± 14	38 ± 6	9 ± 3	55 ± 4	24 ± 4
		Helix Peptide in Water + TFE			
F2	395[a]	45 ± 22	−4 ± 12	40 ± 14	18 ± 13
A5	397 ± 44	45 ± 22	−4 ± 12	40 ± 14	18 ± 13
L7	392 ± 45	45 ± 22	−4 ± 12	40 ± 14	18 ± 13
A8	395 ± 44	45 ± 22	−4 ± 12	40 ± 14	18 ± 13
A10	397 ± 45	45 ± 22	−4 ± 12	40 ± 14	18 ± 13
		Hairpin Peptide in Water			
I3	215[a]	51 ± 32	−12 ± 36	34 ± 33	16 ± 24
T4	215[a]	51 ± 32	−12 ± 36	34 ± 33	16 ± 24
V5	184 ± 67	51 ± 32	−12 ± 36	34 ± 33	16 ± 24
G7	246 ± 87	51 ± 32	−12 ± 36	34 ± 33	16 ± 24
Y10	215[a]	51 ± 32	−12 ± 36	34 ± 33	16 ± 24
		Hairpin Peptide in Water + TFE			
I3	235 ± 41	35 ± 12	4 ± 5	49 ± 7	19 ± 9
T4	247[a]	35 ± 12	4 ± 5	49 ± 7	19 ± 9
V5	247[a]	35 ± 12	4 ± 5	49 ± 7	19 ± 9
G7	247[a]	35 ± 12	4 ± 5	49 ± 7	19 ± 9
Y10	259 ± 44	35 ± 12	4 ± 5	49 ± 7	19 ± 9

[a] Value shown is an average for all residues.

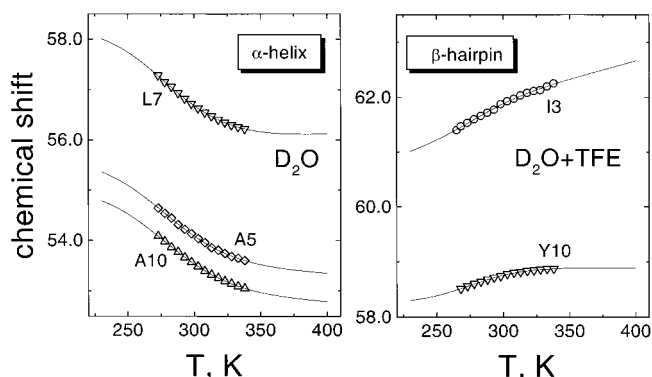

FIGURE 8: The $^{13}C_\alpha$ chemical shift is plotted vs the temperature in K for select residues in helix (left panel) and hairpin (right panel) peptides. Actual data are shown as open symbols, and the solid lines represent fits to these data as described in the text.

lines represent the fits to these data, as described in the Materials and Methods section. With the exception of N-terminal residue F2 in the α-helix peptide, this analysis yielded reasonable values for C_α $\Delta\nu$ (determined at a ^{13}C frequency of 201 MHz) for the peptide in water and in water/ TFE (Table 1). The observed chemical shift difference of about 1−2 ppm is as expected for an α-helix-folding transition (26). For residue F2, the chemical shift data did not show a good inflection over the accessible temperature range; therefore, the fits were poor. For this reason, τ_{ex} for F2 was derived using the simple average of $\Delta\nu$ values for the other residues in the helix peptide.

For the β-hairpin peptide in water, the hairpin−coil transition temperature, T_m, was found to be about 10 °C less than the lowest temperature accessible experimentally. For most residues where a clear inflection was not readily discernible, the low T_m made it difficult to accurately obtain

chemical shift differences and populations. For this reason, $\Delta\nu$ for $^{13}C_\alpha$ could only be determined for V5 and G7 (Table 1), and the average of $\Delta\nu$ for these two residues was used in the analysis of other hairpin residues. For the hairpin peptide in water/TFE, on the other hand, this was not a problem because T_m was significantly higher. However, in this case overlap of carbon resonances with those from TFE was a problem, and $\Delta\nu$ for $^{13}C_\alpha$ could only be determined for I3 and Y10 (Table 1). Therefore, because $\Delta\nu$ values were close to each other in each case (water and water/TFE, respectively) and were consistent with the range usually found in the literature (*28*), $\Delta\nu$ values for C_α were simply averaged and used for the other hairpin residues as listed in Table 1. In fitting any of these chemical shift data using eq 9, only one value for ΔT and T_m was used for all residues in a given peptide in water or in water/TFE (Table 1). This resulted in good fits of the chemical shift data (see Figure 8) and also yielded reasonable values for folded-state populations that were generally consistent with those given in the literature. Average populations for the folded helix peptide, p_h, in water, for example, were found to be $55 \pm 4\%$ at 5 °C and $24 \pm 4\%$ at 30 °C. These values agree well with values determined from circular dichroism measurements: 50% at 5 °C and 20% at 30 °C (*8*). For the helix peptide in water/TFE, p_h at 30 °C was nearly the same as that stated in the literature (*8*), whereas p_h at 5 °C was found to be $40 \pm 14\%$, much less than that of about 85% stated in the literature (*8*). Since our value of 40% seemed low, further analysis to derive τ_{ex} used both this value and that from the literature. Using either value for p_h yielded similar results for τ_{ex} because eqs 4, 5, and 10 are not very sensitive to changes in p_h between about 20% and 80%.

Exchange times, τ_{ex}, were calculated using eq 10 with values for the chemical shift difference, $\Delta\nu$, and populations of folded and unfolded states given in Table 1. For both peptides in water and in water/TFE, τ_{ex} falls within the microsecond time regime (Figure 9) as expected from the probable range for τ_{ex} illustrated in Figure 7. In water, however, τ_{ex} values for both peptides vary from residue to residue from about 0.8 to 5 μs at 30 °C to about 1.5 to 9 μs at 5 °C. Even though this might suggest the presence of a nonglobal exchange process, such a conclusion cannot be made given experimental errors. Moreover, in water/TFE, τ_{ex} values for all labeled sites within each respective peptide are essentially the same from site to site, consistent with the idea that this folding–unfolding exchange process is a global phenomenon. The only exception might be taken as residue F2 in the helix peptide where τ_{ex} at higher temperature deviates greatly from the other residues (A5, L7, A8, and A10). As mentioned above, this deviation may be due to the fact that F2 is positioned at the more mobile N-terminus of the peptide. From the temperature dependence of τ_{ex} (Figure 9), the activation energy, E_a, for folding–unfolding in the helix peptide, averaged over residues in the helix part, can be estimated to be 6 kcal/mol in water and 5 kcal/mol in water/TFE. For the hairpin peptide, average E_a values are 3 kcal/mol in water and 7 kcal/mol in water/TFE. Overall, the activation energy for folding–unfolding is close to the activation energy for the self-diffusion of water, i.e., 4.5 kcal/mol.
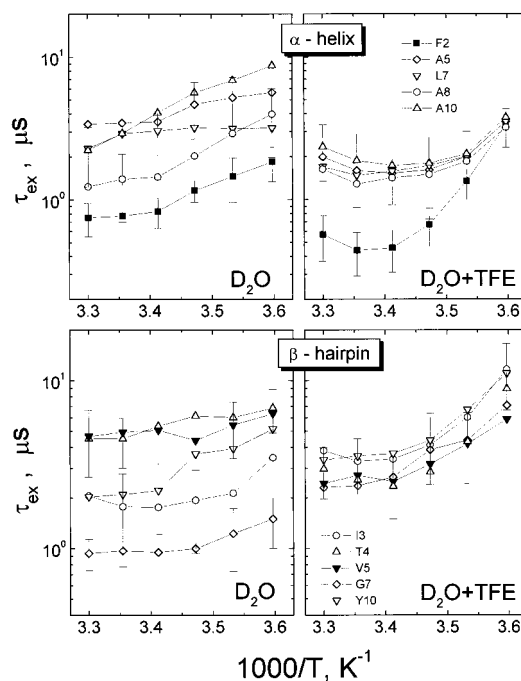

FIGURE 9: Calculated exchange times, τ_{ex}, for $^{13}C_\alpha$ groups are plotted as a function of the inverse temperature in K^{-1} for the α-helix peptide (top panel) and the β-hairpin peptide (bottom panel) in water and in water/TFE. Legends for the symbols identifying residues in each peptide are presented in the figure.

DISCUSSION

For both the α-helix and β-hairpin peptides, an exchange process is occurring on the microsecond time scale. This, however, does not indicate the microscopic mechanism responsible for the observed exchange phenomenon. Three possible mechanisms are aggregation, folding–unfolding, and local conformational rearrangements. Aggregation was ruled out because chemical shifts and line widths did not demonstrate any dependence on peptide concentration and pulsed-field gradient-derived diffusion coefficients indicated the absence of self-association. Local conformational rearrangements, which are known to occur on the microsecond time scale, were a possibility. However, this is more a case for larger, well-folded peptides or proteins where, for example, groups of residues fluctuate simultaneously in segmental motions. For short, linear peptides like those investigated here, internal motions do not occur over groups of residues in a concerted fashion, unless they are linked to folding–unfolding of the peptide. Therefore, the most likely explanation for the observed exchange in these peptides is folding–unfolding. This is supported by several observations. First, when the peptides are more folded as in water/TFE, τ_{ex} values for individual residues in each of these peptides are essentially the same, suggesting the presence of a global process like folding–unfolding. In water, τ_{ex} values for both peptides appear to vary from residue to residue. This is partly due to experimental error. Nonetheless, τ_{ex} values are all within the 0.7–10 μs range. Second, the exchange contribution to T_2 is correlated to changes in the population of folded and unfolded states of the peptides. The exchange contribution to T_2 is maximal at the folded:unfolded population of about 50:50 and decreases as this ratio decreases. Last, this microsecond time scale has been identified with folding–unfolding processes in other small peptides using NMR

relaxation and other experimental techniques. For an alanine-based helix-forming peptide, for example, Thompson et al. (*3*) found that the folding time was about 1 μs. For a 20-residue peptide designed to fold into a monomeric three-stranded antiparallel β-sheet in aqueous solution, the folding time for β-sheet formation was estimated from NMR measurements to be in the range of 4−14 μs at 10 °C (*5*). By using laser flash-induced, rapid thermal denaturation, Munoz et al. (*6*) observed that folding of a 16-residue β-hairpin peptide derived from protein GB1 occurs in about 6 μs at room temperature.

For the derivation of folding−unfolding exchange times, a simple two-state model (folded state and unfolded state) was used. Although this is not unusual and a two-state model is often used, at least to a first approximation, to analyze and to discuss protein and peptide folding−unfolding events, one cannot rule out the possibility for the presence of microsecond time scale exchange among multiple states. In fact, Ramirez-Alvarado et al. (*30*) have found that the unfolded state for this same hairpin peptide contains significant elements of a collapsed state. Therefore, R_{ex} may contain contributions from exchange among folded, unfolded, and collapsed states. In any event, given the experimental errors, it is not possible to distinguish between two-state and multistate exchange, and the use of a more elaborate, multistate folding model would not yield better fits to the data and would only complicate the analysis.

In water/TFE, the folding exchange times, τ_{ex}, were, within error, the same from residue to residue within each respective peptide, helix, and hairpin. For the helix peptide in water/TFE at 5 °C, τ_{ex} falls between 3 and 4 μs for all residues (simple average of 3.4 μs). Not only does this support the idea of a global exchange mechanism for folding but also that use of the two-state model is sufficient to explain the data. At 30 °C, τ_{ex} is also essentially the same for all residues within the helix part of the peptide (simple average of 1.9 μs). However, at 30 °C, τ_{ex} for N-terminal, hydrophobic staple residue F2 was found to be much smaller (about 0.5 μs). In the well-folded state (water/TFE at 5 °C), the helix peptide is more structured with F2 being packed against L7 in the hydrophobic staple (*8*) and the mobility of the N-terminus is reduced, whereas at higher temperature (30 °C), the folded-state population is lower and the N-terminus is more mobile, contributing to a smaller value for τ_{ex}. In terms of the adequacy of using the two-state model, the same can be said with the hairpin peptide for which τ_{ex} values for all residues are, within error, the same (simple average of 8.8 μs at 5 °C and 3.1 μs at 30 °C).

In water alone, however, τ_{ex} varies slightly in some cases from residue to residue for both helix and hairpin peptides. The residue-dependent variability of τ_{ex} with these peptides in water is at least partly due to errors in determining R_{ex} and in estimating populations and chemical shift differences between folded and unfolded states, especially for the hairpin peptide, as indicated by the errors shown for τ_{ex} values. In addition, the presence of broader conformational distributions in folded and unfolded states could contribute to this variation. Peptides in water could exist in structured, collapsed, and random coil states to various extents at different temperatures, and τ_{ex} could be dependent on residue type and position in the sequence and structure. Addition of TFE narrows the conformational distribution

and reduces the spread in τ_{ex} values.

It should be mentioned that some folding and unfolding times given in the literature are unidirectional, i.e., either folding or unfolding times. For example, the room temperature folding time of 6 μs found for the 16-residue β-hairpin peptide derived from protein GB1 (*6*) is for the transition from the unfolded state to the folded state. Exchange times, τ_{ex}, derived from NMR relaxation measurements are average values of folding and unfolding times. Nevertheless, the time scales must be the same in order for R_{ex} contributions to R_2 to be measured. If we define the lifetime in the folded (helix or hairpin) state as τ_f and that in the unfolded (random coil) state as τ_c, then the measured exchange time is actually an average of these two lifetimes:

$$\tau_{ex} = \tau_f \tau_c / (\tau_f + \tau_c) \tag{11}$$

Stabilization of the folded state means that the lifetime of the peptide in the folded state, τ_f, should increase. To have a somewhat larger, or even similar, value for τ_{ex}, the lifetime of the peptide in the unfolded state, τ_c, must decrease. In other words, the folding rate constant should become larger and the unfolding rate constant should become smaller such that the folding equilibrium constant should increase, which it does. In this regard, τ_{ex} for the hairpin peptide measured by NMR, for example, is about the same as that measured by Munoz et al. (*6*) for the folding time of the GB1 β-hairpin peptide.

This study also showed that the folding−unfolding exchange time for the helix peptide in water/TFE is about 2−3-fold less than that for the hairpin peptide, and this difference appears to be even less in water alone. In other words, folding of a helix-forming peptide occurs somewhat faster than the folding of a hairpin-forming peptide. This conclusion is consistent with other studies on peptide folding. As mentioned above, for example, Thompson et al. (*3*) found that the folding time for an alanine-based helix-forming peptide was about 1 μs, whereas the folding time for a comparably sized 20-residue β-hairpin/sheet-forming peptide was estimated to be in the range of 4−14 μs (*5*), as was the folding time for a 16-residue β-hairpin peptide (6 μs) (*6*). The fastest folding time for a helix-forming peptide (21 residues) has been reported to be 0.16 μs at 28 °C (*31*). However, given that rate constants for formation of a single turn of helix generally fall in the time range of 0.1−14 ps (*32*), peptide folding−unfolding should occur on a time scale greater than 0.1 μs.

CONCLUSIONS

NMR spectroscopy has been used to derive exchange contributions to the transverse relaxation rates for individual residues in one helix peptide and in one hairpin peptide. From these data, exchange times were estimated using a two-state folding model and were found to be in microsecond range as observed for folding events with other peptides and consistent with the view that peptide folding occurs on a time scale greater than about 0.1 μs. TFE, which is known to stabilize the conformations of both peptides, had little effect on average exchange times but did significantly narrow the site-to-site variability of exchange times. The difference in folding−unfolding exchange times between these helix and hairpin peptides was found to be, at most, 2−3-fold,

indicating that the folding of short helix-forming peptides occurs only slightly faster than that of hairpin-forming peptides of comparable length.

REFERENCES

1. Becker, E. D. (1980) *High-Resolution NMR. Theory and Chemical Applications*, 2nd ed., Academic Press, New York.
2. Mandel, A. M., Akke M., and Palmer, A. G. (1996) *Biochemistry 35*, 16009−16023.
3. Thompson, P. A., Eaton, W. A., and Hofrichter, J. (1997) *Biochemistry 36*, 9200−9210.
4. Eaton, W. A., Munoz, V., Thompson, P. A., Henry, E. R., and Hofrichter, J. (1998) *Acc. Chem. Res. 31*, 745−753.
5. de Alba, E., Santoro, J., Rico, M., and Jimenez, M. A. (1999) *Protein Sci. 8*, 854−865.
6. Munoz, V., Thompson, P. A., Hofrichter, J., and Eaton, W. A. (1997) *Nature 390*, 196−199.
7. Ramirez-Alvarado, M., Blanco, F. J., and Serrano, L. (1996) *Nat. Struct. Biol. 3*, 604−612.
8. Munoz, V., Blanco, F. J., and Serrano, L. (1995) *Nat. Struct. Biol. 2*, 380−385.
9. Atherton, E, Sheppard, R. C., (1989) *Solid-Phase Peptide Synthesis: A practical approach*, IRL Press, Oxford.
10. Shaka, A. J., Barker, P. B., Freeman, R. (1980) *J. Magn. Reson. 64*, 547−552.
11. Daragan, V. A., Kloczewiak, M. A., and Mayo, K. H. (1993) *Biochemistry 32*, 10580−10590.
12. Farrow, N. A., Muhandiram, R., Singer, A. U., Pascal, S. M., Kay, C. M., Gish, G., Shoelson, S. E., Pawson, T., Forman-Kay, J. D., and Kay, L. E. (1994) *Biochemistry 33*, 5984−6003.
13. Tokuhiro, T., and Fraenkel, G. (1968) *J. Chem. Phys. 49*, 3998−4008.
14. Orekhov, V., Pervushin, K., and Arseniev, A. (1994) *Eur. J. Biochem. 219*, 887−896.
15. Loria, J., Rance, M., and Palmer, A. (1999) *J. Am. Chem. Soc. 121*, 2331−2332.
16. Palmer, A., Skelton, N., Chasin, W., Wright, P., and Rance, M. (1992) *Mol. Phys. 75*, 699−711.
17. Kay, L., Nicholson, L., Delaglio, F., Bax, A., and Torchia, D. (1992) *J. Magn. Reson. 97*, 359−375.
18. Zinn-Justin, S., Berthault, P., Guenneugues, M., and Desvaux, H. (1997) *J. Biomol. NMR 10*, 363−372.
19. Mulder, F., de Graaf, R., Kaptein, R., and Boelens, R. (1998) *J. Magn. Reson. 131*, 351−357.
20. Mayo, K. H., Daragan, V. A., Idiyatullin, D., and Nesmelova, I. (2000) *J. Magn. Reson. 146*, 188−195.
21. Peng, J. W., and Wagner, G. (1994) *Methods Enzymol. 239*, 563−596.
22. Yamazaki, T., Muhandiram, R., and Kay, L. E. (1994) *J. Am. Chem. Soc. 116*, 8266−8278.
23. Millet, O., Loria, J. P., Kroenke, C. D., Pons, M., and Palmer, A. G., III (2000) *J. Am. Chem. Soc. 122*, 2867−2877.
24. Allerhand, A., and Gutowsky, H. S. (1964) *J. Chem. Phys. 41*, 2115−2126.
25. Deverell, C., Morgan, R. E., and Strange, J. H. (1970) *Mol. Phys. 18*, 553−559.
26. Stellwagen, E., and Shalongo, W. (1997) *Biopolymers 43*, 413−418.
27. Ishima, R., and Torchia, D. A. (1999) *J. Biomol. NMR 14*, 369−372.
28. Wishart, D. S., and Sykes, B. D. (1994) *Methods Enzymol. 239*, 363−392.
29. Ramirez-Alvarado, M., Blanco, F. J., Niemann, H., and Serrano, L. (1997) *J. Mol. Biol. 273*, 898−912.
30. Ramirez-Alvarado, M., Daragan, V. A., Serrano, L., and Mayo, K. H. (1998) *Protein Sci. 7*, 720−729.
31. Williams, S., Causgrove, T. P., Gilmanshin, R., Fang, K. S., Callender, R. H., Woodruff, W. H., and Dyer, R. B. (1996) *Biochemistry 35*, 691−697.
32. Gruenewald, B., Nicola, C. U., Lustig, A., Shwartz, G., and Klump, H. (1979) *Biophys. Chem. 9*, 137−147.